

Highly heterogeneous depleted mantle recorded in the lower oceanic crust

Sarah Lambert^{1,2*}, Janne M. Koornneef³, Marc-Alban Millet¹, Gareth R. Davies³, Matthew Cook¹ and C. Johan Lissenberg¹

The Earth's mantle is heterogeneous as a result of early planetary differentiation and subsequent crustal recycling during plate tectonics. Radiogenic isotope signatures of mid-ocean ridge basalts have been used for decades to map mantle composition, defining the depleted mantle endmember. These lavas, however, homogenize via magma mixing and may not capture the full chemical variability of their mantle source. Here, we show that the depleted mantle is significantly more heterogeneous than previously inferred from the compositions of lavas at the surface, extending to highly enriched compositions. We perform high-spatial-resolution isotopic analyses on clinopyroxene and plagioclase from lower crustal gabbros drilled on a depleted ridge segment of the northern Mid-Atlantic Ridge. These primitive cumulate minerals record nearly the full heterogeneity observed along the northern Mid-Atlantic Ridge, including hotspots. Our results demonstrate that substantial mantle heterogeneity is concealed in the lower oceanic crust and that melts derived from distinct mantle components can be delivered to the lower crust on a centimetre scale. These findings provide a starting point for re-evaluation of models of plate recycling, mantle convection and melt transport in the mantle and the crust.

The mantle, Earth's largest geochemical reservoir and main source of volcanism, records the time-integrated history of recycling of oceanic lithosphere and its overlying sediments during the plate tectonic cycle^{1,2}. The resulting compositional heterogeneity generated within the mantle reflects this recycling process^{3,3}. Determining the magnitude and length scale of this heterogeneity will enable a reconstruction of the recycling process and mantle convection, ultimately providing a window onto the dynamics of our planet. Mid-ocean ridge basalts (MORBs) have been the primary tool to map the geochemical heterogeneity of the oceanic upper mantle for decades³⁻⁵. However, because MORBs mix in crustal magma chambers^{6,7}, the degree to which they are representative of the mantle source remains poorly constrained. Hence, the true heterogeneity of the MORB mantle source is uncertain, providing a significant barrier to understanding the magnitude and scale of recycled crust and the long-term evolution of the mantle.

One approach is to analyse the isotopic compositions of abyssal peridotites. These mantle samples may preserve a wider range of isotopic compositions than associated lavas⁷⁻¹⁴. However, they represent the melting residue of the MORB source, and potentially could have therefore lost the most fusible material¹⁰ (pyroxenite, eclogite) thought to represent recycled, enriched, components¹. Furthermore, interpretations are complicated by the common occurrence of recent refertilization in the lithospheric mantle beneath the ridge axis¹¹⁻¹³ and severity of alteration^{7,11}.

In this study, we overcome this problem by conducting crystal-scale Nd and Sr isotopic analyses on primitive cumulate minerals from the lower oceanic crust, and show that these cumulate minerals crystallized from heterogeneous melts extending to significantly more enriched compositions than the associated MORB.

Substantial small-scale heterogeneity in cumulate minerals

This study focuses on the Mid-Atlantic Ridge (MAR) segment north of the Atlantis Transform Fault (30° N), which is predominantly

composed of volcanic rocks with isotopically depleted, normal MORB compositions¹⁵. Along the ridge–transform intersection, an uplifted dome of ultramafic and mafic plutonic rocks exposed by detachment faulting (the Atlantis Massif¹⁶) provides a window into the lower oceanic crust. Drill core of gabbroic cumulates (Integrated Ocean Drilling Program, IODP, hole U1309D) yielded a detailed, 1,415 m record of the lower crust¹⁶, which, along with the associated volcanic rocks, provides a unique opportunity to compare the isotopic heterogeneity of melts delivered to the lower crust with those erupted onto the seafloor. Results of Nd (¹⁴³Nd/¹⁴⁴Nd) and Sr (⁸⁷Sr/⁸⁶Sr) isotopic analyses on individual microdrilled clinopyroxene and plagioclase crystal domains from plutonic rocks of hole U1309D are shown in Fig. 1. We compare these data with whole-rock isotopic compositions of diabase and microgabbros collected on the same core, associated basalt flows (IODP sites U1310 and U1311) and Atlantic MORB and abyssal peridotite data from the literature in Figs. 1 and 2.

The results indicate that cumulate minerals (1) are significantly more isotopically heterogeneous than the associated diabase and lavas, exceeding the range of ¹⁴³Nd/¹⁴⁴Nd in MORB from 30° N by a factor of seven (Fig. 1), (2) capture a significant proportion of mantle heterogeneity reported in abyssal peridotites (Fig. 2a,b) and (3) record almost the full Nd isotopic heterogeneity currently observed in all North Atlantic MORB (including the enriched, plume-influenced Azores platform, Iceland and Jan Mayen; Fig. 2a,b). Furthermore, Nd isotopic heterogeneity occurs down to the centimetre scale, with plagioclase and clinopyroxene from individual samples commonly not in isotopic equilibrium (Fig. 3). This small-scale heterogeneity can be explained by multiple replenishments in the crystal mush leading to dissolution–crystallization episodes¹⁷ and juxtaposition of diverse populations of crystals¹⁸. At the grain scale, cores show more primitive compositions (higher Mg# [=Mg/(Mg+Fe), molar] in clinopyroxene and anorthite content in plagioclase) than rims (Supplementary Fig. 1), suggesting that the cores

¹Cardiff University, School of Earth and Ocean Sciences, Cardiff, UK. ²University of Utah, Department of Geology and Geophysics, Salt Lake City, USA.

³Vrije Universiteit, Faculty of Science, Amsterdam, The Netherlands. *e-mail: sarah.lambart@utah.edu

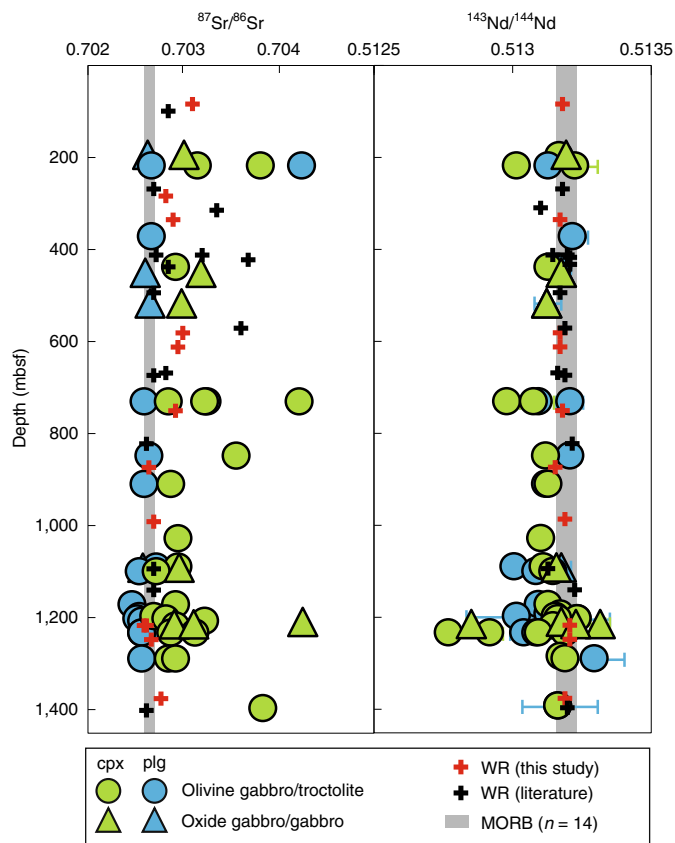


Fig. 1 | Isotopic compositions of Atlantis Massif cumulate minerals.

$^{87}\text{Sr}/^{86}\text{Sr}$ and $^{143}\text{Nd}/^{144}\text{Nd}$ ratios of clinopyroxene (cpx) and plagioclase (plg) cores of cumulate gabbroic rocks from IODP hole U1309D, compared with whole-rock (WR) isotopic analyses performed in this study and on gabbroic rocks recording less than 40% alteration⁴². The grey bands represent the compositional variability of MORB analysed in this study and reported in the literature (PetDB database⁴³) at the same latitude ($30^\circ \text{N} \pm 1^\circ$). Error bars: 2 SE (standard error of the mean); mbfsf, metres below seafloor.

crystallized from primitive melts during melt emplacement in the crust, while rims crystallized from late-stage percolating melts¹⁹. Once minerals have formed, Nd diffusion is too slow to destroy grain-scale heterogeneity: at the solidus temperature of a gabbro, Nd zoning is preserved in calcic plagioclase on a $100\ \mu\text{m}$ scale for more than 10 Myr (ref. 20); diffusion of Nd in clinopyroxene is even slower²¹.

$^{87}\text{Sr}/^{86}\text{Sr}$ ratios are similarly variable. Most plagioclase data fall on the Sr–Nd isotopic data array defined by global MORB (Supplementary Fig. 2) and could conceivably represent primary values. However, clinopyroxenes typically record higher $^{87}\text{Sr}/^{86}\text{Sr}$ than plagioclase, suggesting that seawater alteration may have overprinted mantle signatures. Hence, we use only Nd isotope data for the interpretation.

A *t*-test shows no statistical difference between clinopyroxene and plagioclase $^{143}\text{Nd}/^{144}\text{Nd}$, but together the cumulate minerals represent a distinct population compared with basalt, diabase and microgabbros ($P < 0.0002$). However, the mean whole-rock $^{143}\text{Nd}/^{144}\text{Nd}$ of the diabase, microgabbros and associated basalt flows (0.513198 ± 41) is within the 2σ error of that of the cumulate minerals (0.513138 ± 187). Thus, there is no difference in the average compositions of the cumulate minerals relative to the basalt, diabase and microgabbros, but cumulate minerals record a larger variability.

This indicates that cumulate minerals represent products of crystallization of small amounts of melt that have undergone limited mixing before being delivered to the crust, whereas erupted MORBs represent averages of much higher volumes of magmas that have been significantly mixed together at shallower depths.

Depleted mantle composition and temperature variations

These findings have important implications for both the magnitude and the scale of heterogeneity of the upper mantle. The striking similarity of the Nd isotopic frequency distribution of cumulate minerals at Hole U1309D with that of North Atlantic MORB as a whole (Fig. 4) indicates that mantle heterogeneity beneath the Atlantis Massif is representative of the magnitude of heterogeneity in the North Atlantic basin. It follows that it is the proportion of recycled material in the aggregated magma, rather than the degree of isotopic enrichment of the recycled material in the source, that is responsible for variations in MORB isotopic compositions. If so, along-axis MORB variations should record the proportion of each component in MORB and in the mantle source along the axis. To assess this hypothesis, we use an adiabatic mantle melting model²² to calculate (1) the required proportion of melt derived from recycled material to reproduce the Nd isotopic ratio of North Atlantic MORB (Methods), (2) the corresponding fraction of recycled material in the mantle source and (3) the thickness of oceanic crust generated along the ridge axis. It has been suggested that MORB at the scale of a ridge segment (that is, $\sim 300\ \text{km}$) experienced common differentiation processes²³. Hence, we used the weighted average MORB compositions at a segment scale. The melt derived from the recycled material has a higher Nd abundance than depleted peridotitic melt¹¹. Hence, adding a small amount of depleted peridotitic melt to the melt derived from recycled material does not significantly affect the isotopic composition of the latter. Conversely, even a small contribution of melt derived from recycled material can significantly modify the isotopic composition of the depleted peridotite melt in such a way that the isotopic signature of the depleted component is unlikely to be preserved in the cumulate minerals (Methods). Hence, we used the most enriched composition recorded in cumulates ($^{143}\text{Nd}/^{144}\text{Nd} = 0.512800 \pm 15$) and the most depleted composition recorded in North Atlantic abyssal peridotites ($^{143}\text{Nd}/^{144}\text{Nd} = 0.513662 \pm 18$)⁷ as isotopic compositions of the mantle endmembers. Assuming that the enriched material is represented by recycled oceanic crust²⁴ (Methods), the calculation yields a proportion of melt derived from recycled material in locally averaged MORB of 27–59% (Fig. 2c). This proportion is a function of both the proportion of recycled material in the source and the mantle potential temperature (Supplementary Fig. 6a). To convert the proportion of melt derived from recycled material in MORB to a proportion of recycled material in the mantle we performed three sets of calculations: (1) we fixed the mantle potential temperature to $T_p = 1,300^\circ\text{C}$ and calculated the fraction of recycled material in the source required to explain the melt compositions, (2) we fixed the fraction of recycled material in the mantle at 4% (that is, the average fraction estimated in the first set of calculations) and calculated the T_p required to explain the melt compositions and (3), in a hybrid model, we varied both the proportion of recycled material and the mantle potential temperature. These calculations also yield melt volume, and hence crustal thickness. To evaluate the validity of these models we compare the calculated crustal thickness for each ridge segment with its average seafloor depth, a proxy for crustal thickness²⁵ (Fig. 2d and Supplementary Fig. 6b–e).

Varying the mantle potential temperature alone clearly failed to match the elevation profile, creating negative thickness anomalies around the major hotspots and producing crustal thickness variations much larger than those observed in the Atlantic basin²⁶. Furthermore, it required a large range of mantle potential temperatures (1180 – 1440°C). It is worth noting, however, that varying the

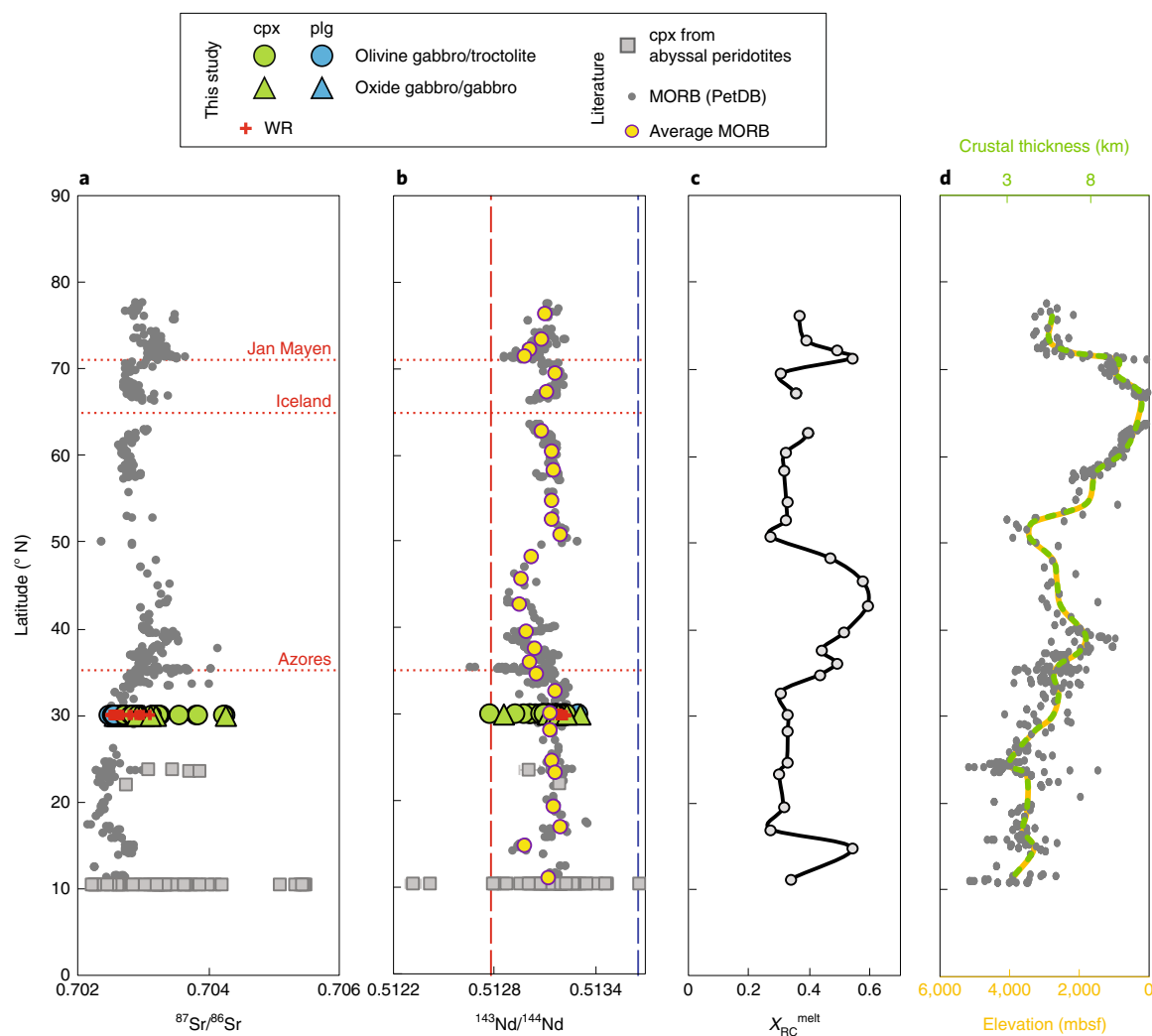


Fig. 2 | Isotopic compositions of cumulate minerals, abyssal peridotites and MORBs along the northern MAR and results of geochemical modelling. **a, b**, $^{87}\text{Sr}/^{86}\text{Sr}$ (**a**) and $^{143}\text{Nd}/^{144}\text{Nd}$ (**b**) ratios measured in this study, in MORB (PetDB Database⁴³) and in abyssal peridotites^{71,213} from the northern MAR. Red dotted lines show the latitudes of the major hotspots affecting MORB compositions¹⁵. Error bars: 2SE. In **b**, the vertical dashed lines show the isotopic compositions of the two mantle components used in calculations and the yellow circles are the average MORB compositions per ridge segment. **c**, Calculated fraction of melt derived from recycled material in the averaged MORB. **d**, Comparison of the calculated crustal thicknesses generated by varying the proportion of recycled material and the potential temperature (dashed green line) with the averaged elevations of the collected MORB (orange line).

potential temperature of a heterogeneous mantle can create a negative correlation between the contribution of the pyroxenite in the melt (Fig. 2c) and the crustal thickness (Supplementary Fig. 6b), as observed for the Vema lithospheric section¹². Varying the proportion of recycled material alone did not reproduce small-scale elevation variations on ridge segments far from the hotspots²⁷. It also did not reproduce the bathymetry anomaly centred on Iceland. This anomaly is attributed to a significantly thickened crust (>10 km)²⁶, probably produced by higher mantle potential temperature or high melt flux²⁸. However, large-scale variations, such as the higher elevations of Jan Mayen and the Azores platform, are overall better correlated with thickness variations due to small variations of proportions of recycled material in the source rather than with thickness variations due to temperature variations. The best match is obtained with the hybrid model. Considering a variation of crustal thickness between 3 and 11 km (ref. ²⁶), both compositional and elevation profiles are reproduced by varying T_p between 1,245 and 1,367 °C and the proportion of recycled material in the source between 3.2 and 8.5% (Fig. 2d and Supplementary Fig. 6d,e). Hence,

our calculations support a model where a higher proportion of recycled material in the source around the hotspot creates clear crustal thickness and chemical anomalies along most of the northern MAR without requiring large (>120 °C) thermal variations.

Limited magma mixing during melt transport in the mantle

The finding of high-magnitude mantle heterogeneity delivered to the crust down to the centimetre scale requires that the MORB source is heterogeneous on a length scale smaller than the melting region. Variations of melt production have been observed along the northern MAR on a scale of 25–50 km (ref. ²⁹). If this length scale of variation is due to various proportions of mantle components in the source region, then the scale of individual compositional domains must be smaller. Short (10^{-3} to 10^{-2} m) Nd (and Sr) isotopic heterogeneity can persist over timescales of 10^9 yr in the solid mantle³⁰. However, short-scale mantle heterogeneities decrease the likelihood of extracting the melt in (chemical) isolation, and melt–solid diffusion may destroy the isotopic signatures. Hence, our study supports the prevalence of a kilometre-scale length scale of heterogeneity in the MORB mantle source^{12,31}.

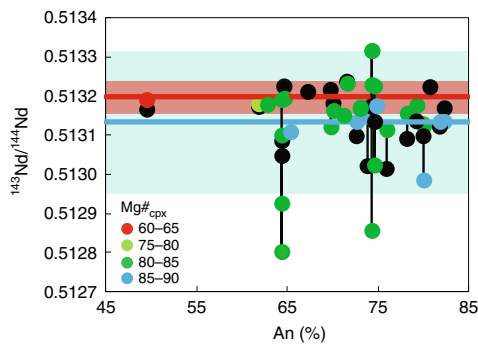


Fig. 3 | Intrasample heterogeneity. $^{143}\text{Nd}/^{144}\text{Nd}$ ratios of plagioclase (black circles) and clinopyroxene (coloured circles) as a function of the anorthite (An) content of the plagioclase in the sample. Analyses from individual samples are connected by black tie lines. The blue line and field show the average and 2σ composition of the cumulate minerals. The red line and field show the average composition and 2σ of MORB (basalts, diabase and microgabbros).

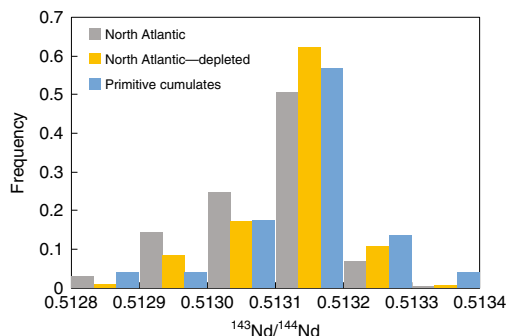


Fig. 4 | Frequency distribution of Nd isotopic compositions. Comparison between plagioclase and clinopyroxenes from primitive cumulates (this study) and North Atlantic MORB (grey, all data; yellow, MORB not affected by hotspots³⁵).

Crucially, the isotopic heterogeneity we observe in the Atlantis Massif cumulate minerals provides strong evidence that heterogeneous melts are delivered to the lower crust without significant mixing. Most melt generated by decompression melting is considered to be extracted from the mantle through high-permeability channels^{32,33}. It has previously been argued that channelized melt transport is accompanied by significant mixing³¹. However, if this were the case, it would quickly dilute heterogeneous isotopic compositions. Hence, our results suggest that magma mixing inside the channels is limited. We propose that each mantle component could generate its own network of channels to account for both preservation of isotopic heterogeneities and rapid magma transport³⁴ (Fig. 5). Melt–rock reactions between melt derived from recycled material and subsolidus peridotite favour a (near) closed-system evolution^{35,36}, and thermal diffusion can nucleate channelization that preferentially samples melts from the most fusible component^{37,38}. Eventually, magmas from the less fusible adjacent mantle can also start to focus together through reactive or mechanical instabilities^{30,33}. Such processes would discourage mixing between magmas derived from each component and preserve extreme isotopic compositions (Fig. 5).

In conclusion, the isotopic heterogeneity revealed in the lower oceanic crust provides strong evidence that the limited isotopic variability recorded in MORB is a consequence of crustal-level

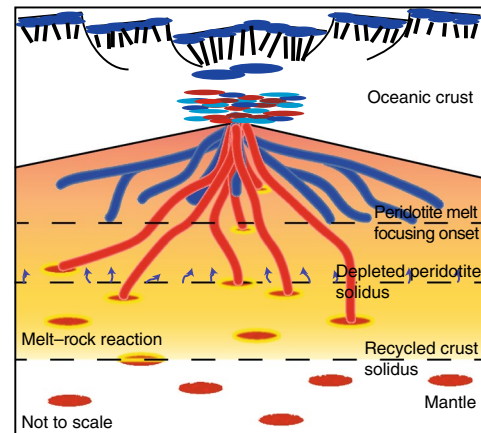


Fig. 5 | Illustration of magma delivery from a two-component mantle to the crust. The fusible and enriched recycled material starts to melt at higher pressure than the depleted peridotite and reacts with the surrounding mantle (red and yellow ovals). The recycled material and depleted peridotite nucleate their own networks of high-permeability channels (in red and blue, respectively), facilitated by melt–rock reaction^{35,36} and thermal diffusion^{37,38}, and by mechanical³⁰ and/or chemical³³ instabilities, respectively. Generation of separate networks limits magma mixing and helps to deliver a larger isotopic variability to the crust. The shallowest axial magma chamber hosts a larger volume of magma, where mixing and crystallization continue, resulting in the loss of much of the primary mantle diversity.

mixing of melts from a highly heterogeneous source. Furthermore, our novel analytical approach offers considerable potential to assess the full heterogeneity delivered to the crust across a range of geodynamics settings. Finally, these new findings require re-evaluations of models for convective thinning and stretching during mantle convection^{39,40} and for melt migration through the mantle and the crust^{31,41} to account for greater isotopic heterogeneity and limited magma mixing in the depleted mantle.

Online content

Any methods, additional references, Nature Research reporting summaries, source data, statements of code and data availability and associated accession codes are available at <https://doi.org/10.1038/s41561-019-0368-9>.

Received: 10 September 2018; Accepted: 12 April 2019;

Published online: 20 May 2019

References

- Allègre, C. J. & Turcotte, D. L. Implications of a two-component marble-cake mantle. *Nature* **323**, 123–127 (1986).
- Hofmann, A. W. Mantle geochemistry: the message from oceanic volcanism. *Nature* **385**, 219–229 (1997).
- Hart, S. R. Heterogeneous mantle domains: signatures, genesis and mixing chronologies. *Earth Planet. Sci. Lett.* **90**, 273–296 (1988).
- White, W. M. Sources of oceanic basalts: radiogenic isotopic evidence. *Geology* **13**, 115–118 (1985).
- Cohen, R. S., Evensen, N. M., Hamilton, P. J. & O’Nions, R. K. U–Pb, Sm–Nd and Rb–Sr systematics of mid-ocean ridge basalt glasses. *Nature* **283**, 149–153 (1980).
- Batiza, R. Inverse relationship between Sr isotope diversity and rate of oceanic volcanism has implications for mantle heterogeneity. *Nature* **309**, 440–441 (1984).
- Cipriani, A., Brueckner, H. K., Bonatti, E. & Brunelli, D. Oceanic crust generated by elusive parents: Sr and Nd isotopes in basalt–peridotite pairs from the Mid-Atlantic Ridge. *Geology* **32**, 657–660 (2004).
- Stracke, A. et al. Abyssal peridotite Hf isotopes identify extreme mantle depletion. *Earth Planet. Sci. Lett.* **308**, 359–368 (2011).
- Warren, J. M. Global variations in abyssal peridotite compositions. *Lithos* **248**, 193–219 (2016).

10. Salters, V. J. M. & Dick, H. J. B. Mineralogy of the mid-ocean-ridge basalt source from neodymium isotopic composition of abyssal peridotites. *Nature* **418**, 68–72 (2002).
11. Warren, J. M., Shimizum, N., Sakaguchi, C., Dick, H. J. B. & Nakamura, E. An assessment of upper mantle heterogeneity based on abyssal peridotite isotopic compositions. *J. Geophys. Res. Solid Earth* **114**, B12203 (2009).
12. Brunelli, D., Cipriani, A. & Bonatti, E. Thermal effects of pyroxenites on mantle melting below mid-ocean ridges. *Nat. Geosci.* **11**, 520–525 (2018).
13. Mallick, S., Dick, H. J., Sachi-Kocher, A. & Salters, V. J. Isotope and trace element insights into heterogeneity of subridge mantle. *Geochem. Geophys. Geosyst.* **15**, 2438–2453 (2014).
14. Snow, J. E., Hart, S. R. & Dick, H. J. B. Nd and Sr isotope evidence linking mid-ocean-ridge basalts and abyssal peridotites. *Nature* **371**, 57–60 (1994).
15. Gale, A., Dalton, C. A., Langmuir, C. H., Su, Y. & Schilling, J. G. The mean composition of ocean ridge basalts. *Geochem. Geophys. Geosyst.* **14**, 489–518 (2013).
16. Blackman, D. K. et al. Drilling constraints on lithospheric accretion and evolution at Atlantis Massif, Mid-Atlantic Ridge 30°N. *J. Geophys. Res.* **116**, B07103 (2011).
17. Leuthold, J. et al. Partial melting of lower oceanic crust gabbro: constraints from poikilitic clinopyroxene primocrysts. *Front. Earth Sci.* **6**, 15 (2018).
18. Schleicher, J. M. & Bergantz, G. W. The mechanics and temporal evolution of an open-system magmatic intrusion into a crystal-rich magma. *J. Petrol.* **58**, 1059–1072 (2017).
19. Lissenberg, C. J. & MacLeod, C. J. A reactive porous flow control on mid-ocean ridge magmatic evolution. *J. Petrol.* **57**, 2195–2220 (2016).
20. Cherniak, D. J. REE diffusion in feldspar. *Chem. Geol.* **193**, 25–41 (2003).
21. Van Orman, J. A., Grove, T. L. & Shimizu, N. Rare earth element diffusion in diopside: influence of temperature, pressure, and ionic radius, and an elastic model for diffusion in silicates. *Contrib. Mineral. Petrol.* **141**, 687–703 (2001).
22. Lambart, S. No direct contribution of recycled crust in Icelandic basalts. *Geochem. Perspect. Lett.* **4**, 7–12 (2017).
23. Shorttle, O. Geochemical variability in MORB controlled by concurrent mixing and crystallization. *Earth Planet. Sci. Lett.* **424**, 1–14 (2015).
24. Hart, S., Blusztajn, J., Dick, H. J. B., Meyer, P. S. & Muehlenbachs, K. The fingerprint of seawater circulation in a 500-meter section of ocean crust gabbros. *Geochim. Cosmochim. Acta* **63**, 4059–4080 (1999).
25. Barth, G. A. & Mutter, J. C. Variability in oceanic crustal thickness and structure: multichannel seismic reflection results from the northern East Pacific Rise. *J. Geophys. Res.* **101**, 17951–17975 (1996).
26. Wang, T., Lin, J., Tucholke, B. & Chen, Y. J. Crustal thickness anomalies in the North Atlantic Ocean basin from gravity analysis. *Geochem. Geophys. Geosyst.* **12**, Q0AE02 (2011).
27. Langmuir, C. H., Klein, E. M. & Plank, T. Petrological systematics of mid-ocean ridge basalts: constraints on melt generation beneath ocean ridges. *Geophys. Monogr. Ser.* **71**, 183–280 (1992).
28. MacLennan, J. Concurrent mixing and cooling of melts under Iceland. *J. Petrol.* **49**, 1931–1953 (2008).
29. Wang, T., Tucholke, B. E. & Lin, J. Spatial and temporal variations in crustal production at the Mid-Atlantic Ridge, 5°N–27°30'N and 0–27 Ma. *J. Geophys. Res. Solid Earth* **120**, 2119–2142 (2015).
30. Kogiso, T., Hirschmann, M. M. & Reiners, P. W. Length scales of mantle heterogeneities and their relationship to ocean island basalt geochemistry. *Geochim. Cosmochim. Acta* **68**, 345–360 (2004).
31. Liu, B. & Liang, Y. The prevalence of kilometer-scale heterogeneity in the source region of MORB upper mantle. *Sci. Adv.* **3**, e1701872 (2017).
32. Kelemen, P. B., Shimizu, N. & Salters, V. J. M. Extraction of mid-ocean-ridge basalt from the upwelling mantle by focused flow of melt in dunite channels. *Nature* **375**, 747–753 (1995).
33. Spiegelman, M., Kelemen, P. B. & Aharonov, E. Causes and consequences of flow organization during melt transport: the reaction infiltration instability in compactible media. *J. Geophys. Res.* **106**, 2061–2077 (2001).
34. Elliott, T. & Spiegelman, M. in *Treatise on Geochemistry* 2nd edn (eds Holland, H. D. & Turekian, K. K.). 543–581 (Elsevier, 2014).
35. Lambart, S., Laporte, D., Provost, A. & Schiano, P. Fate of pyroxenite-derived melts in the peridotitic mantle: thermodynamical and experimental constraints. *J. Petrol.* **53**, 451–476 (2012).
36. Yaxley, G. & Green, D. H. Reactions between eclogite and peridotite: mantle refertilisation by subduction of oceanic crust. *Schweiz. Mineral. Petrogr. Mitt.* **78**, 243–255 (1998).
37. Weatherley, S. M. & Katz, R. F. Melting and channelized magmatic flow in chemically heterogeneous, upwelling mantle. *Geochem. Geophys. Geosyst.* **13**, Q0AC18 (2012).
38. Weatherley, S. M. & Katz, R. F. Melt transport rates in heterogeneous mantle beneath mid-ocean ridges. *Geochim. Cosmochim. Acta* **172**, 39–54 (2016).
39. Anderson, D. L. The scales of mantle convection. *Tectonophysics* **284**, 1–17 (1998).
40. Stixrude, L. & Lithgow-Bertelloni, C. Geophysics of chemical heterogeneity in the mantle. *Annu. Rev. Earth Planet. Sci.* **40**, 569–595 (2012).
41. Wanless, V. D. & Shaw, A. M. Lower crustal crystallization and melt evolution at mid-ocean ridges. *Nat. Geosci.* **5**, 651–655 (2012).
42. Delacour, A., Früh-Green, G. L., Frank, M., Gutjahr, M. & Kelley, D. S. Sr- and Nd-isotope geochemistry of the Atlantis Massif (30°N, MAR): implications for fluid fluxes and lithospheric heterogeneity. *Chem. Geol.* **254**, 19–35 (2008).
43. Lehnert, K., Su, Y., Langmuir, C., Sarbas, B. & Nohl, U. A global geochemical database structure for rocks. *Geochem. Geophys. Geosyst.* **1**, 1012 (2000).

Acknowledgements

This work was supported by the European Union's Horizon 2020 research and innovation programme (Marie Skłodowska-Curie grant agreement No. 663830) and National Science Foundation (EAR-1834367) to S.L. and by the award NERC NE/R001332/1 to M.-A.M. We thank D. Muir, I. McDonald, T. Oldroyd and M. Jansen for their assistance on the scanning electron microscope, with LA-ICP-MS, with sample preparation and in using the micromill, respectively.

Author contributions

C.J.L. designed the study. S.L. and C.J.L. wrote the manuscript with input from M.-A.M., J.M.K. and G.R.D. S.L. and C.J.L. selected the samples. S.L. and M.C. performed the element maps. S.L. performed trace element analyses and geochemical modelling. S.L. and C.J.L. performed micromilling, and S.L., C.J.L., M.-A.M. and J.M.K. performed column chemistry and isotopic analyses.

Competing interests

The authors declare no competing interests.

Additional information

Supplementary information is available for this paper at <https://doi.org/10.1038/s41561-019-0368-9>.

Reprints and permissions information is available at www.nature.com/reprints.

Correspondence and requests for materials should be addressed to S.L.

Publisher's note: Springer Nature remains neutral with regard to jurisdictional claims in published maps and institutional affiliations.

© The Author(s), under exclusive licence to Springer Nature Limited 2019

Methods

Geological setting and sample selection. The Atlantis Massif is a 1.5–2 Myr old oceanic core complex on the western rift flank of the MAR at 30° N. IODP sites U1309, U1310 and U1311 were drilled during expeditions 304 and 305. The main hole, hole U1309D, penetrated 1415.5 mbsf and recovery averaged 75%. Over 96% of hole U1309D is made up of gabbroic rock types, which are amongst the most primitive as well as freshest plutonic rocks known from the ocean floor¹⁶.

We selected 74 samples from the core U1309D samples to cover the entire drill hole, including 28 olivine gabbros, 8 troctolites, 7 olivine-rich troctolites, 11 gabbros, 4 oxide gabbros, 2 gabbro-norites, 6 microgabbros and 7 diabases. We also collected 9 basalt and glass samples recovered at IODP sites U1310 and U1311.

Element maps and selection of mineral for isotopic analyses. Forty of the selected samples were polished and carbon coated to perform major and minor element maps. Element maps were obtained at Cardiff University on a Zeiss Sigma HD field emission gun scanning electron microscope equipped with dual Oxford Instruments X-max 150 mm² energy-dispersive silicon drift detectors. We used an acceleration voltage of 20 kV and a dwell time of 9 ns. The beam current and aperture were adjusted to obtain optimum output count rates of about 410,000 counts per second, enabling rapid mapping of large proportions of the samples at high spatial resolution (step size 20 µm). Raw counts were background corrected using Oxford Instruments' AZtec software, which was then used to generate multi-element maps.

From these element maps, we selected primitive, fracture- and inclusion-free, plagioclase (high anorthite content) and clinopyroxene (high Mg# and low TiO₂/Cr₂O₃ ratio) cores for micromilling (Supplementary Fig. 1). We also preferentially selected large minerals to limit the depth of each drill hole and the number of holes required to collect enough material for Nd isotopic analysis. Finally, we carefully examined every selected drilling area for fractures or inclusions and redefined the drilling area accordingly.

LA-ICP-MS measurements and estimations of the Nd and Sr content of the sample. We determined trace element concentrations on the selected clinopyroxenes and plagioclases using laser ablation inductively coupled plasma mass spectrometry (LA-ICP-MS). Analyses were performed at Cardiff University on a New Wave Research UP213 UV laser system attached to a Thermo X Series 2 ICP-MS. Each mineral underwent two analyses (by lines) to allow mineral compositional variability to be assessed. A minimum length of 300 µm and a beam diameter of 80 µm were used, with a laser operating at 10 Hz frequency and sample translation at 6 µm s⁻¹. Acquisition time was about 80 s (20 s gas blank, >50 s acquisition, 10 s washout).

We used the silicate glass standard NIST 612 as a reference material, and clinopyroxene and plagioclase Ca contents, measured by scanning electron microscopy energy-dispersive spectroscopy, served as an internal standard. We tested the accuracy of the measurement with two external standards (BIR and BCR-2G) analysed every 10 samples. Based on 10 BRC-2G measurements, the relative errors on the trace element contents lie between 0.3 and 15%, with 3.8 and 5.2% for Nd and Sr respectively (Supplementary Fig. 3).

Microsampling with micromill. Micromilling of the samples was performed in the Faculty of Sciences at Vrije Universiteit Amsterdam and in the School of Earth and Ocean Sciences at Cardiff University. We used a procedure adapted from that described by Charlier et al.⁴¹ for thick sections. Polished billets were first placed in an ultrasonic bath of Milli-Q water (standard purity with a final resistivity of >18.4 MΩ) for 20 min, and then cleaned with acetic acid for 1 min and finally cleaned and dried with ethanol. Drill bits were also cleaned between sampling in 0.165 M HCl for 2 s and then in an ultrasonic bath of Milli-Q water for 10 min.

We placed two or three drops of Milli-Q water on the area to be drilled. The drilled material is suspended as the drilling proceeds. When the solution became saturated, it was pipetted into a Teflon vial previously cleaned for isotope chemistry and new drops of Milli-Q water were added to the drilling area. During the whole drilling procedure, we made sure that Milli-Q water was always present. Finally, at the end of the drilling sequence, all the water on the sample was collected.

After the micromilling was complete, we estimated the sampled volume by measuring the surface area and the depth of the hole. We also checked for the presence of inclusions. This gave us a maximum estimate of the volume of material collected, as not all the drilled material is recovered.

Total procedural blanks were performed by simulating a 60 min milling sequence on a clean sample. A clean drill bit was immersed into Milli-Q water on the rock slab sample, and the water was collected and resupplied following the same procedure as a regular micromilling sequence to collect a similar amount of water. The blanks were then processed by column chemistry following the same procedure as for the samples (see below).

Column chemistry. Separation of Sr and Nd from plagioclase and clinopyroxene cores. Column chemistry on plagioclase and clinopyroxene powders was performed at Vrije Universiteit Amsterdam and in the CELTIC laboratory at Cardiff University. Samples were dissolved in Teflon vials in a 4:1 mix of HF and HNO₃ on a hotplate at 140 °C for 3 d. Sr and rare earth elements (REEs) were separated from

the matrix in a setup whereby Sr resin columns (Eichrom, 50 µl resin) are placed directly above TRU resin columns (Eichrom, 150 µl resin). By placing the Sr resin column above the TRU resin column during loading and washing, the pre-fraction from the Sr column (in 3 M HNO₃) was directly eluted onto the TRU column, after which the two column sets were separated and Sr and REEs were eluted. Finally, the Nd was further separated from the other REEs in a Ln resin column procedure (see Fig. 5 of Koornneef et al.⁴³ for details). Due to the large sample size needed for Nd isotope analyses for plagioclase, most Sr plagioclase samples were subjected to a second pass of Sr chemistry.

Total procedural blanks varied between 38 and 43 pg for Sr and 2 and 12 pg for Nd. The blanks were determined by isotope dilution using an ⁸⁶Sr spike and a ¹⁵⁰Nd spike respectively.

Separation of Sr and Nd on whole rock. We performed whole-rock isotopic analyses on six diabase samples, five microgabbros and one olivine-rich troctolite from core U1309D, as well as on eight basalts and one basaltic glass recovered from IODP sites U1310 and U1311. Column chemistry was performed in the CELTIC laboratory at Cardiff University. Samples were crushed into an agate ball mill grinder and we collected between 200 and 300 mg. All but the glass sample (1310-A1-13-19) were leached in hot 6 M HCl for 3 h and then rinsed to remove unbonded Sr (ref. ⁴⁶). The glass powder was leached at room temperature in 6 M HCl for 30 min. After centrifugation of the samples, the supernatant was discarded and samples were washed in Milli-Q water, centrifuged again and the supernatant again discarded. Residual powders were then digested in hot concentrated HNO₃ and HF for 24 h, dried down, taken up in 1 ml of concentrated HNO₃ and dried down again before being redissolved in 8 M HNO₃ and centrifuged.

Sr was separated in a double pass through a 1 ml pipette-tip column containing Sr-spec resin. Samples were loaded in 8 M HNO₃ and sample matrix (including Ca and Rb) was removed in the same acid. Sr was then collected in 0.05 M HNO₃ (ref. ⁴⁷). Samples were dried again and sequentially dissolved in concentrated HNO₃ and HCl, refluxed on a hotplate for at least 24 h and finally dried down prior to being dissolved dilute HCl.

Nd was separated in two steps. The REEs were first separated from the sample matrix using columns filled with a cation exchange resin (BioRad AG50W-x8, 2.5 ml). The REE fraction was then dried and Nd was separated using columns filled with Ln-spec resin (Eichrom, 1.1 ml)⁴⁸.

Total procedural blanks were 10 and 15 pg for Sr and Nd, respectively.

Mass spectrometry. Clinopyroxene and plagioclase samples. Sr and Nd analyses on plagioclase and clinopyroxene cores were performed on a Thermo Scientific TRITON Plus TIMS at Vrije Universiteit Amsterdam. Samples and standards were loaded on outgassed Re filaments in a clean air flow unit. Strontium analyses were performed using annealed Re filaments in a single-filament setup, whereas for Nd analyses annealed and zone-refined Re filaments were used in a double-filament configuration for the evaporation and ionization positions, respectively^{45,49}. Isotope analyses were performed using 10¹¹ Ω amplifiers in the feedback loop of the Faraday detectors. Six of the current amplifiers installed in the TRITON Plus at VU Amsterdam have the conventional 10¹¹ Ω resistors, whereas the other four amplifiers are equipped with 10¹³ Ω resistors. The Sr and Nd collection measurements reported here were carried out with the same static analytical approach as used by Koornneef et al.⁴⁹.

The estimated amounts of Nd and Sr analysed, as well as the number of cycles for each analysis, are reported in Supplementary Table 1. An 11 min baseline was measured during heating of the sample and subtracted online from the raw intensity values. In most cases, analyses were run to exhaustion. On average, we acquired 194 and 214 cycles for Sr isotopic analyses in plagioclase and clinopyroxenes, respectively, and 85 and 97 cycles for Nd isotopic analyses in plagioclase and clinopyroxene, respectively.

For Sr analyses, the intensity on the 87 mass was corrected for minor ⁸⁷Rb contributions using the canonical ⁸⁷Rb/⁸⁶Rb of 0.3857. During Nd analyses, Sm was not detected for all but three clinopyroxenes (149R2-68-71a, 252R4-3-6a and 257R1-95-100a). For the three clinopyroxenes where we detected ¹⁴⁷Sm we correct the 144 intensity using ¹⁴⁴Sm/¹⁴⁷Sm = 0.20502. Nd and Sr measurements are subsequently corrected for instrumental mass fractionation using the exponential law, and ¹⁴⁶Nd/¹⁴⁴Nd = 0.7219 and ⁸⁶Sr/⁸⁸Sr = 0.1194, respectively. To test the accuracy of the measurements, 7–8 mg of BHVO-2 standards were passed through the complete chemical procedure. Filaments were loaded with either 2 or 10 ng of Nd, and with 200 ng of Sr. Data are within the error of the preferred values reported in the GeoReM database (Supplementary Fig. 4).

Whole rock. Sr and Nd isotope ratios were measured on a Nu Instruments multicollector ICP-MS system in the CELTIC laboratory at Cardiff University in static mode. Sr isotopic measurements were normalized internally to ⁸⁶Sr/⁸⁸Sr = 0.1194, and NBS-987 was run every five samples as a secondary correction to account for small variations in non-exponential mass bias. ⁸⁶Kr interferences were below background level, therefore no correction was made. Nd isotopic measurements were normalized internally to ¹⁴⁶Nd/¹⁴⁴Nd = 0.7219 and JNd-i was run every five samples as a secondary correction to account for small variations in non-exponential mass bias. The accuracy of the measurements

was tested using JB-2 as a secondary standard that was passed through the complete chemical procedure, and the Sr and Nd isotopic ratios obtained are indistinguishable within error from the preferred values reported in the GeoReM database (Supplementary Fig. 5).

Calculation of contribution of recycled material to parental melts and fraction of recycled-material-derived melt in parental melts. For the enriched component, we used the isotopic ratio of the most enriched clinopyroxene analysed in this study ($^{143}\text{Nd}/^{144}\text{Nd} = 0.512800 \pm 15$; $^{87}\text{Sr}/^{86}\text{Sr} = 0.702884 \pm 9$). Such an isotopic signature can be reproduced by partial melting of an approximately 1.1 Ga recycled gabbro⁵⁰ (Supplementary Fig. 2). We used the same major and trace element composition as used to calculate the age, that is the average oceanic gabbro composition estimated by Hart et al.²⁴. For the depleted component, we used the isotopic ratio of the most depleted abyssal peridotite reported along the MAR (Vema lithospheric section⁷, $^{143}\text{Nd}/^{144}\text{Nd} = 0.51366$) and major and trace element compositions of the depleted endmember of the depleted MORB mantle (D-DMM; ref. 51). To estimate the fractions of each endmember in the parental melts of cumulate minerals, we need to know the Nd content of melt generated by each endmember. Following the approach used by Lambert²², we considered that the mantle follows an adiabatic path, with $T_p = 1,300^\circ\text{C}$. Both components are in thermal equilibrium and chemically isolated. We used Melt-PX (ref. 52) to calculate the pressure (P)–temperature (T)–melt fraction (F) path. We considered that both lithologies were chemically isolated but in thermal equilibrium. Calculations performed with Melt-PX take into account heat transfer between the different lithologies. Calculations were stopped when the mantle column had upwelled to the base of the crust, that is, when the pressure at the base of the crust $P_c = P$. The initial fraction of recycled gabbro in the mantle source (that is, 5%) was chosen such that a 5–6 km crust thickness was generated²⁹. We used alphaMELTS (ref. 53) to calculate the mineral assemblage at each pressure step (that is, every 100 bar) for each lithology. We calculated the Nd content of the melt derived from each lithology along the adiabatic path using incremental batch melting calculations, integrating the liquid produced over the melting region and dividing by the total volume produced (see Lambert²² for details of calculations). Accumulated Nd contents of the melt derived from the recycled crust ($[\text{Nd}]_{\text{RC}}$) and D-DMM ($[\text{Nd}]_{\text{DDMM}}$) are 8.1 and 2.7 ppm, respectively. We can solve for the fraction of recycled crust (F_{RC}) required to explain the isotopic mineral compositions, for example

$$\begin{aligned} {}^{143}\text{Nd}/{}^{144}\text{Nd}_{\text{cpx/plg}} &= (F_{\text{RC}} \times [\text{Nd}]_{\text{RC}}) / (F_{\text{RC}} \times [\text{Nd}]_{\text{RC}} + (1 - F_{\text{RC}}) \\ &\quad \times [\text{Nd}]_{\text{DDMM}}) \times {}^{143}\text{Nd}/{}^{144}\text{Nd}_{\text{RC}} \\ &\quad + (1 - F_{\text{RC}} \times [\text{Nd}]_{\text{RC}}) \\ &\quad / (F_{\text{RC}} \times [\text{Nd}]_{\text{RC}} \\ &\quad + (1 - F_{\text{RC}}) \times [\text{Nd}]_{\text{DDMM}}) \\ &\quad \times {}^{143}\text{Nd}/{}^{144}\text{Nd}_{\text{DDMM}} \end{aligned}$$

Nature of the enriched component. As noted above, we assumed that the lowest $^{143}\text{Nd}/^{144}\text{Nd}$ ratio is produced by partial melting of an approximately 1.1 Ga recycled gabbro⁵⁰. However, other processes can produce similar isotopic ratios, such as a small contribution of recycled sediments⁵⁰ or the partial melting of hybrid lithologies resulting from the mixture between older recycled material and peridotite. The contribution of sediments is accompanied by strong enrichments in $^{87}\text{Sr}/^{86}\text{Sr}$ and $^{176}\text{Hf}/^{177}\text{Hf}$, which are difficult to reconcile with the observed MORB array⁵⁰. To investigate the effect of the nature of the enriched material on our calculations, we performed an additional set of calculations using a hybrid lithology, produced by a 1:1 mix between recycled gabbro and depleted peridotite. We used KG1 (ref. 54) for the major element composition and calculated the trace element composition as a 1:1 mixture between the oceanic gabbro⁵⁴ and D-DMM⁵¹. The most enriched clinopyroxene Nd isotopic ratio can be reproduced assuming the recycled gabbro is about 1.3 Ga (ref. 50). The calculated Nd content of the accumulated melt derived from KG1 is 3.8 ppm. Solving for the fraction of KG1 in the melt, we obtained significantly higher (48–75%) contribution of KG1-derived melt in the aggregated magma. Using the estimated fraction of KG1 in the melt, we calculated the corresponding fraction in the source. We can then estimate the proportion of recycled crust in the mantle simply by using the relationship $X_{\text{RC}}^{\text{source}} = 0.5X_{\text{KG1}}^{\text{source}}$. The two calculations produce similar profiles of thickness variation (Supplementary Fig. 6c). However, for $T_p = 1300^\circ\text{C}$, calculations using KG1 yield a proportion of recycled crust between 9 and 21% (Supplementary Fig. 6e). These estimations are significantly higher than previous estimations for the amount of recycled crust in the mantle source of MORB^{55,56}. In summary, the enriched signature can reflect either the direct participation of crustal material (that is, by partial melting) or its indirect participation (by interaction with the

surrounding peridotite and subsequent melting of an ‘enriched’ peridotite/hybrid lithology). However, because of the higher solidus temperatures of peridotite or hybrid lithology such as KG1 in comparison to the recycled crust⁵¹, the proportion of enriched material in the mantle required to reproduce the enriched melt composition is significantly higher in the latter case, resulting in a higher initial proportion of recycled crust needed to produce this enriched composition.

Condition for the preservation of the mantle component isotopic signatures.

The recycled crust has a higher melt productivity⁵³ and Nd abundance²⁴ than the peridotite⁵¹. Hence, even a small degree of mixing will dilute the signature of the most depleted component. Inversely, a small contribution of depleted peridotite melt to the recycled crust-derived melt will not significantly affect the isotopic composition of the latter, and aggregated melts are more likely to sample the enriched endmember composition. In fact, 14% of recycled crust-derived melt in the aggregated magma is required to change the Nd isotopic ratio of the melt from 0.51366 to 0.51332 (that is, from the most depleted abyssal peridotite⁷ to the most depleted cumulate mineral). However, a 14% addition of peridotite melt to the recycled crust-derived melt would only change its isotopic ratio from 0.51280 to 0.51283 (that is, unchanged within error). Hence, while the isotopic composition of the depleted endmember is most likely to be diluted, the most enriched composition observed in cumulate minerals is a good representative of the enriched endmember in the mantle beneath the Atlantis Massif.

Data availability

The data supporting the findings of this study are available within the Article and the Methods and in the PetDB data repository (http://www.earthchem.org/petdbWeb/search/readydata/MAR555-52N_major_trace_isotope.csv).

Code availability

The code used to calculate adiabatic melting of a two-component mantle source, Melt-PX (ref. 52), can be accessed at <https://doi.org/10.1002/2015JB012762>.

References

- Charlier, B. L. A. et al. Methods for the microsampling and high-precision analysis of strontium and rubidium isotopes at single crystal scale for petrological and geochronological applications. *Chem. Geol.* **232**, 114–133 (2006).
- Koornneef, J. M. et al. TIMS analysis of Sr and Nd isotopes in melt inclusions from Italian potassium-rich lavas using prototype 10^{13} Ω amplifiers. *Chem. Geol.* **397**, 14–23 (2015).
- Millet, M. –A., Doucelance, R., Schiano, P., David, K. & Bosq, C. Mantle plume heterogeneity versus shallow-level interactions: a case study, the São Nicolau Island, Cape Verde archipelago. *J. Volcanol. Geotherm. Res.* **176**, 265–276 (2008).
- McGee, L. E., Smith, I. E., Millet, M. –A., Handley, H. K. & Lindsay, J. M. Asthenospheric control of melting processes in a monogenetic basaltic system: a case study of the Auckland Volcanic Field, New Zealand. *J. Petrol.* **54**, 2125–2153 (2013).
- McCoy-West, A. J., Millet, M. –A. & Burton, K. W. The neodymium stable isotope composition of the silicate Earth and chondrites. *Earth Planet. Sci. Lett.* **480**, 121–132 (2017).
- Koornneef, J. M., Bouman, C., Schwieters, J. B. & Davies, G. R. Use of 10^{13} ohm current amplifiers in Sr and Nd isotope analyses by TIMS for application to sub-nanogram samples. *J. Anal. Spectrom.* **28**, 749–754 (2013).
- Stracke, A., Bizimis, M. & Salters, V. J. M. Recycling oceanic crust: quantitative constraints. *Geochem. Geophys. Geosyst.* **4**, 8003 (2003).
- Workman, R. K. & Hart, S. R. Major and trace element composition of the depleted MORB mantle (DMM). *Earth Planet. Sci. Lett.* **231**, 53–72 (2005).
- Lambart, S., Baker, M. B. & Stolper, E. M. The role of pyroxenite in basalt genesis: Melt-PX, a melting parameterization for mantle pyroxenites between 0.9 and 5 GPa. *J. Geophys. Res. Solid Earth* **121**, 5708–5735 (2016).
- Smith, P. M. & Asimow, P. D. Adibat_1ph: a new public front-end to the MELTS, pMELTS, and pHMELTS models. *Geochem. Geophys. Geosyst.* **6**, Q02004 (2005).
- Kogiso, T., Hirose, K. & Takahashi, E. Melting experiments on homogeneous mixtures of peridotite and basalt: application to the genesis of ocean island basalts. *Earth Planet. Sci. Lett.* **162**, 45–61 (1998).
- Hirschmann, M. M. & Stolper, E. M. A possible role for garnet pyroxenite in the origin of the ‘garnet signature’ in MORB. *Contrib. Mineral. Petrol.* **124**, 185–208 (1996).
- Sobolev, A. V. et al. The amount of recycled crust in sources of mantle derived melts. *Science* **316**, 590–597 (2007).